RESEARCH PAPER

Electrochemical detection of the neurotransmitter glutamate and the effect of the psychotropic drug riluzole on its oxidation response

Tao Yu[1] · Jingjie Cui[1] · Shaowei Chen[2]

Abstract

Glutamate is the main excitatory neurotransmitter in the brain and plays a leading role in degenerative diseases, such as motor neuron diseases. Riluzole is a glutamate regulator and a therapeutic drug for motor neuron diseases. In this work, the interaction between glutamate and riluzole was studied using cyclic voltammetry and square-wave voltammetry at a glassy carbon electrode (GCE). It was shown that glutamate underwent a two-electron transfer reaction on the GCE surface, and the electrochemical detection limits of glutamate and riluzole were 483 µmol/L and 11.47 µmol/L, respectively. The results confirm that riluzole can promote the redox reaction of glutamate. This work highlights the significance of electrochemical technology in the sensing detection of the interaction between glutamate and related psychotropic drugs.

Keywords Glutamate · Riluzole · Electrochemical detection · Redox

Introduction

With the rapid development of the global economy and society, mental illness has become an increasingly important factor affecting human life and health [1, 2]. Research has shown that glutamate, as the most abundant endogenous neurotransmitter in the central nervous system, reaches concentrations of 6–7 mM in the synaptic cleft, and in the whole brain it can reach a concentration of 10,000–12,000 µmol/L [3]. Glutamate is closely related to neuronal excitability, prominence, learning, and memory formation. Therefore, physiological dysfunction of glutamate and its receptors is closely related to the onset of mental illness [4–8]. Glutamate in cerebrospinal fluid is derived from the conversion and synthesis of glucose in the central nervous system. There is a dynamic equilibrium in the concentration of glutamate in the human body under normal physiological conditions. When the concentration of glutamate deviates from the normal physiological concentration, a high glutamate concentration will cause continuous activation of its receptors, which will lead to nerve cell damage and oxidative stress [2, 9]. Therefore, glutamate can be used as a biomarker for the diagnosis of Alzheimer's disease and other neurodegenerative diseases, such as amyotrophic lateral sclerosis, stroke, and traumatic brain injury [10–13].

The exogenous glutamate in the blood mainly comes from excessive use of seasonings. Many studies in recent years have shown that obesity, metabolic disorders, neurotoxicity, and reproductive toxicity are related to the overuse of sodium glutamate in chicken essence, soy sauce, and other condiments [6]. A large amount of sodium glutamate intake causes an increase in glutamate concentration in body fluids, which then act on glutamate receptors in the nerve center, disrupting the normal physiological function of neurons, with possible adverse effects on behavior, especially in infants with an underdeveloped blood–brain barrier.

At present, in addition to conventional biochemical detection methods, scientists have been committed to developing new detection methods for glutamate, including capillary electrophoresis [14–18], optical methods [19–21], and electrochemical methods [22–30]. Electrochemical methods have become a major direction of development in recent years due to their advantages of low cost, high specificity, and easy operation. Currently, electrochemical technology
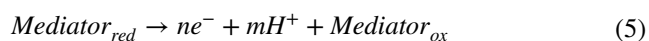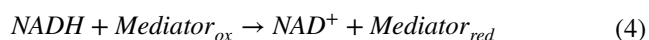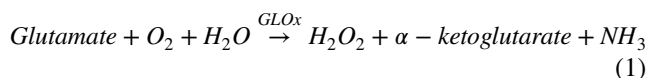
✉ Jingjie Cui
cuijingjie@hdu.edu.cn

1   School of Automation, Hangzhou Dianzi University, Hangzhou 310018, China

2   Department of Chemistry and Biochemistry, University of California, 1156 High Street, Santa Cruz, CA 95064, USA

mainly relies on the specificity of enzyme catalysis to detect glutamate [24–28]. Glutamate oxidase (GLOx) and glutamate dehydrogenase (GLDh) are two important enzymes commonly used in the electrochemical detection of glutamate. The mechanism driving the enzymatic action of GLOx is shown in Eqs. (1) and (2). Under the action of GLOx, glutamate is oxidized by O_2 to α-ketoglutaric acid and produces H_2O_2. H_2O_2 is decomposed in Eq. (2) to release O_2 to achieve molecular balance. Notably, the mechanism of GLOx detection is through the detection of hydrogen peroxide in Eq. (1). However, in aqueous media, oxygen reduction reaction is inevitable [31], and hydrogen peroxide is formed in this process. That is, for GLOx detection, part of the hydrogen peroxide formed by oxygen reduction is not oxidized by GLOx, which results in inaccurate detection results for GLOx. Additionally, the structural stability of the electrode will be damaged as O_2 gas is released (Eq. 2) on the surface of the sensing electrode.

The enzymatic mechanism of GLDh action is represented by Eqs. (3)–(5), where Eq. (3) is the conversion of glutamate to α-ketoglutaric acid under the action of NAD^+. Equations (4) and (5) describe the conversion process between NAD^+ and NADH [26–30]. Unlike GLOx, the catalytic process of GLDh does not involve O_2 and H_2O_2, but achieves the conversion of glutamate and α-ketoglutaric acid through the mutual conversion of NAD^+ and NADH. Therefore, the glutamate dehydrogenase-modified electrode mainly detects glutamate indirectly by detecting NADH generated by Eq. (3) [28]. GLDh-modified electrodes have the disadvantages of a complex manufacturing process and poor sensitivity—for example, the sensitivity of the oxidase-modified electrode constructed by Maity [24] was 723.08 μA cm^{-2} mM^{-1}, while the sensitivity of the dehydrogenase-modified electrode constructed by Martínez-Periñán [28] was only 0.2 μA cm^{-2} mM^{-1}.

$$Glutamate + O_2 + H_2O \overset{GLOx}{\rightarrow} H_2O_2 + \alpha-ketoglutarate + NH_3 \tag{1}$$

$$H_2O_2 \rightarrow 2H^+ + O_2 + 2e^- \tag{2}$$

$$Glutamate + NAD^+ \overset{Gldh}{\rightarrow} NADH + \alpha-ketoglutarate \tag{3}$$

$$NADH + Mediator_{ox} \rightarrow NAD^+ + Mediator_{red} \tag{4}$$

$$Mediator_{red} \rightarrow ne^- + mH^+ + Mediator_{ox} \tag{5}$$

It has been reported that glutamate can be detected by electrochemical methods, and studies have demonstrated the reaction mechanism of glutamate in the presence of enzymes. However, to the best of our knowledge, there has been no report on the reaction mechanism under

electrochemical conditions without enzymes. The use of a stable electrode is essential for studying the redox mechanism of glutamate under electrochemical conditions. In addition to high stability, the glassy carbon electrode (GCE) possesses hardness, superior air tightness, excellent conductivity, biocompatibility, ease of renewal, and good sensitivity, thus offering advantages over other electrodes for electrochemical sensing detection in aqueous media [32].

Riluzole is a benzothiazole type neuroprotective agent with anticonvulsant effects, which is capable of glutamate regulation and antiepileptic and neuroprotective effects [33]. The serum concentration of riluzole is approximately 3.19 μmol/L [34]. It is typically used as a glutamate release inhibitor for the treatment of motor neuron diseases, such as amyotrophic lateral sclerosis [33–37]. Among its many uses, riluzole plays a major role in vivo in inhibiting the release of glutamate, the uptake of the glutamate receptor on the neurotransmitter glutamate, and the expression of the glutamate transporter (EAAT2) [38–42]. In addition, a large number of studies have shown that riluzole has good therapeutic effects in the central nervous system and plays an important role in the treatment of cerebral ischemia [43], spinal cord injury [44, 45], traumatic brain injury [46], Parkinson's disease [47, 48], and other diseases. However, no studies have reported whether an interaction between glutamate and riluzole occurs under electrochemical conditions. Therefore, electrochemical studies of the direct interactions between glutamate and riluzole are critical for understanding the metabolism of drugs and the control of drug side effects.

In this work, a GCE was used as the sensing electrode, and voltammetry and other electrochemical methods were used to study the electrochemical oxidation mechanism of glutamate and riluzole at physiological concentrations, and to determine the mechanism of riluzole with respect to glutamate oxidation under electrochemical conditions.

Experimental

Materials

Glutamate (≥ 99.5%), riluzole (98%), and phosphate-buffered saline (0.1 M PBS; pH 7.4) were obtained from Macklin (Shanghai, China). In our work, 40 mM glutamate and 1 mM riluzole were prepared in ultrapure water as stock solutions, and kept in a cool, dark place.

Electrochemistry

Electrochemical measurements were conducted in a three-electrode configuration, using a GCE as the working electrode, with a geometric area of 0.07 cm^2 (Tianjin Aida Hengsheng Technology Co., Ltd.). A platinum wire was

used as the auxiliary electrode and Ag/AgCl (saturated KCl) was used as the reference electrode. In all experiments, 0.1 M PBS (pH 7.4) was used as the electrolyte. Experimental data were collected using a CHI660C electrochemical workstation (Shanghai Chenhua Instrument Co., Ltd). A pH meter (Shunkeda, China) was used to measure the solution pH. Before conducting the experiment, the GCE was sequentially polished with 1.0 μm and 0.3 μm Al_2O_3 slurry to obtain a good mirror surface, and was then electrochemically cleaned and activated by cyclic voltammetry (scanning rate of 100 mV/s, potential range of −0.1 V to 1.8 V) in 0.5 M dilute sulfuric acid until a steady cyclic voltammogram was obtained. The treated electrode was stored in a cool, clean place until use. All data in this work were processed using OriginPro software.

Results and discussion

Electrochemical detection of glutamate

GLOx and GLDh enzyme-modified electrodes only detect glutamate indirectly, which can affect the detection results in aqueous media. Here, the GCE was used for direct detection of glutamate. Cyclic voltammetry (CV) was used to detect 9.8 mM Glu solution at a scanning rate of 100 mV/s, and the results are shown in Fig. 1a. It can be seen that in the potential range of $-0.6\ V \leq E_{app} \leq 1.2\ V$, the glutamate sample showed an oxidation peak of 3.24 μA at 0.33 V and a reduction peak of −2.86 μA at 0.22 V, compared to the blank voltammogram in Fig. 1a. In addition, in order to further verify that these two peaks are the detection peaks of Glu, square-wave voltammetry (SWV) was used to detect Glu at a detection potential of −0.1 V to 1.1 V (Fig. 1b). Compared to the blank square-wave voltammogram, it can be seen that the oxidation peak at 0.33 V in the positive scan (green curve) and the reduction peak at 0.22 V in the negative scan (red curve) are in agreement with the results of CV (Fig. 1a). Therefore, it is preliminarily determined that the redox peaks at 0.33 V and around 0.22 V are

the characteristic detection peaks of Glu on the surface of the GCE, which is basically consistent with the glutamate potential results reported in the literature [49]. The origin of these glutamate redox peaks will be further discussed in the following section, "Electrode kinetics of glutamate." Additionally, in Fig. 1a, the CV curve after glutamate was added showed a reduction peak of −11.77 μA at −0.46 V. This peak can be attributed to the reduction of dissolved oxygen to $HO_2^{•}$ and OH^- in glutamate aqueous solution [50, 51].
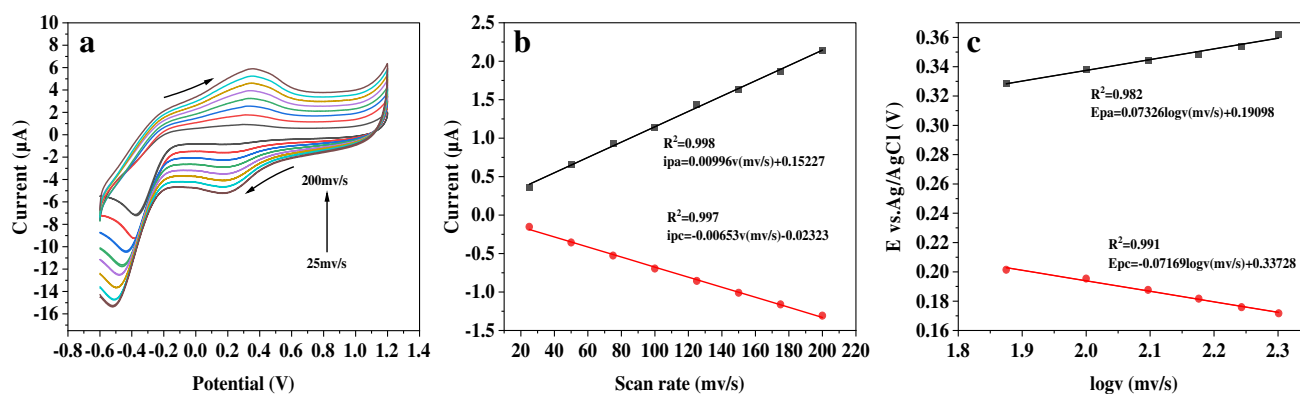
Electrode kinetics of glutamate

In order to explore the mechanism of its reaction, an in-depth study was conducted on the glutamate (Glu) redox dynamics. We performed CV detection of Glu using the same electrode at a scanning rate of 25–200 mV/s (Fig. 2). Figure 2a shows the cyclic voltammograms of Glu at different scanning speeds. It can be seen that the potential difference (ΔE_P) increased from 0.076 V to 0.177 V as the scan rate was increased from 25 mV/s to 200 mV/s, indicating that the electrochemical reaction of glutamate on the GCE is a quasi-reversible reaction. The relationship between peak current and scanning rate is shown in Fig. 2b, which reveals that the redox peak current exhibits a linear relationship with the scanning rate. The linear fitting equation for the oxidation reaction is $Ip_a = 0.1523 + 0.001v$ (mV/s), and $R(8)^2 = 0.998$, and the linear fitting equation for the reduction reaction is $Ip_c = -0.0232 - 0.0065v$ (mV/s), $R(8)^2 = 0.997$; in these equations, s is defined as the scan rate. The above results show good linearity between the sweep rate and peak current, and demonstrate that the electro-oxidation of glutamate on the GCE surface is controlled by adsorption, so the kinetic parameters can be calculated by the Laviron equation [52]:

$$Epc = -\frac{2.3\,RT}{\alpha nF}\log v + constant \qquad (6)$$

Fig. 1 Electrochemical voltammetry detection of 9.8 mM glutamate in 0.1 M PBS solution (pH = 7.4): (**a**) CV detection with a scanning rate 100 mV/s, potential range −0.6 V to 1.2 V; (**b**) SWV detection with positive scan (green curve, potential range 0–1.1 V) and negative scan (red curve, potential range −0.1 V to 1 V), $E_s = 4$ mV, pulse amplitude 0.025 V, f = 4 Hz
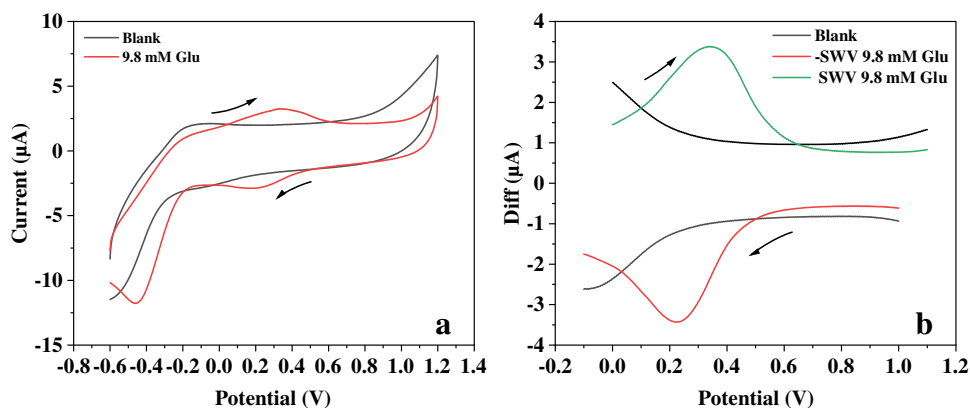
Fig. 2 Electrode kinetic studies of glutamate: (**a**) cyclic voltammetric detection of 9.8 mM Glu in PBS (pH = 7.4) at different scan rates, potential range −0.6 V to 1.2 V; (**b**) linear fitting plot between peak current and scan rate; (**c**) linear fitting plot between the logarithm of the peak potential of the redox peak and the scanning rate

$$Epa = \frac{2.3\,RT}{(1-\alpha)nF}\log v + constant \tag{7}$$

where R is the ideal gas constant 8.314 J/(mol K), T is 293 K, F is the Faraday constant 96,485 C/mol, α is the electron transfer coefficient, and n is the number of reaction electrons. Figure 2c establishes the redox peak potential (Epa, Epc) and the logarithm of the scan rate (log v). The linear relationship between the cathode process and the anode process is as follows:

$$Epc = -0.07169logv + 0.33728 \; (R^2 = 0.991) \tag{8}$$

$$Epa = 0.07326logv + 0.19098 \; (R^2 = 0.982) \tag{9}$$

Based on Eqs. (6) and (7), the values of α and n are 0.51 and 1.6 ($\approx$ 2), respectively. It can be concluded that the Glu redox under the action of the electric field may be a double-electron transfer reaction.

## Electro-oxidation mechanism of glutamate

It is well established that a glutamate molecule contains one amino group and two carboxyl groups, so the glutamate solution is acidic. In this work, we obtained the number of transferred electrons of glutamate electro-oxidation by experimental calculation, and the pH of the glutamate solution was observed in the range of 3.5–4.3 during the electrochemical detection process. It has been reported that the oxidation process of Glu mainly involves the conversion of α-ketoglutaric acid [9]. According to the above calculated electron transfer number and the literature reported, it may be inferred that the electro-oxidation mechanism of glutamate mainly includes the following steps (Scheme 1). First, combining a proton with lone pairs of N, the amino group (–NH₂) of glutamate forms a positively charged ammonium

salt a, and then loses one electron for deamination reaction to generate glutamate positive ion b [53]. The carbonyl oxygen on 1C strongly attracts electrons, which causes a significant lack of electrons in 2C. The ortho transfer of an electron-rich atom forms a double-bond glutaric acid positive ion c. Then c forms d by hydroxylation in acidic media. The enol structure in d is unstable, and is finally transformed into α-ketoglutaric acid [54].

Sensitivity of glutamate detection

In order to determine the glutamate (Glu) detection sensitivity, SWV was used to detect low concentrations (0.9–3 mM) of Glu (as shown in Fig. 3a), and the linear relationship between the oxidation peak current and the natural logarithm of the concentration of Glu (lnc) is shown in Fig. 3b. A good linear relationship can be seen between the natural logarithm of the concentration of Glu and the oxidation peak current. The linear equation is Ip_a (μA) = 0.965lnc (mmol/L) + 1.961, R^2 = 0.994, where its slope is defined as the sensitivity coefficient (N) of the sensor; the sensitivity can be obtained by the ratio of N to the electrode surface area, and the sensitivity of the GCE to glutamate reaches 13.66 μAcm^{-2} mM^{-1}. The limit of detection (LOD) calculation formula uses the concentration of Glu corresponding to $Ip_a = Ip_{a0} + 3S$, where S is the standard deviation of the oxidation peak current for 10 blank PBS solution detections, and Ip_{a0} is the average current value at 0.33 V for 10 blank PBS solution detections. After detection, $Ip_{a0} = 1.19 \times 10^{-6}$ A and S = 2.39 × 10^{-8} A, so Ip_a is 1.26 × 10^{-6} A, substituting the value of Ip_a into the concentration logarithmic current fitting curve. In this work, the detection limit is calculated to be 483 μmol/L, and the detection limit is less than 6 mM [3, 55]. Therefore, the electrochemical detection of glutamate using the GCE can achieve detection under physiological concentration conditions, and

Scheme 1 Electrochemical oxidation mechanism of glutamate on the surface of the glassy carbon electrode
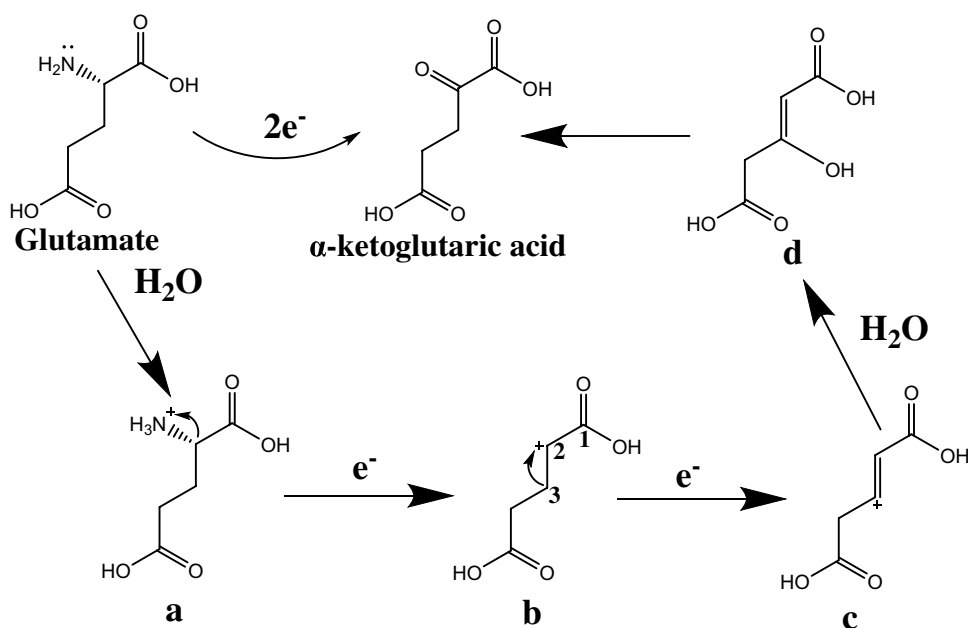
Fig. 3 (**a**) SWV detection curve of different concentrations of glutamate in PBS solution (pH = 7.4), potential range 180–680 mV, E_s = 4 mV, pulse amplitude 0.025 V, f = 4 Hz; (**b**) plot of the relationship between peak current and glutamate concentration
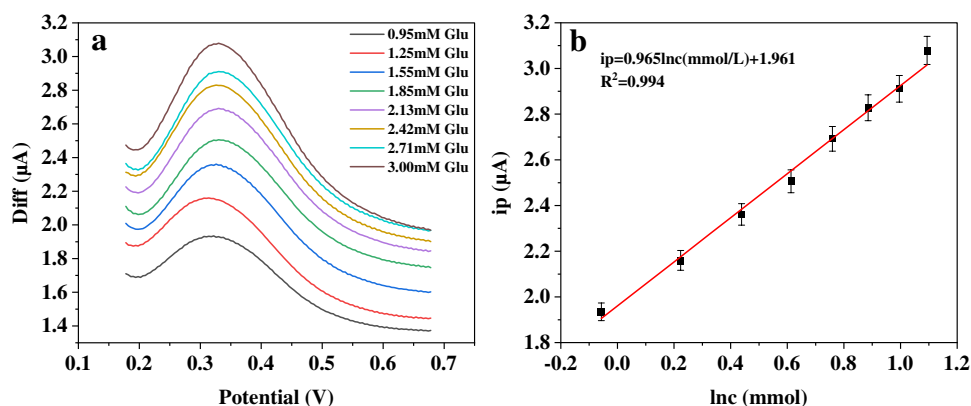
with the use of GCEs, the electrochemical system has higher stability than with enzyme electrodes.
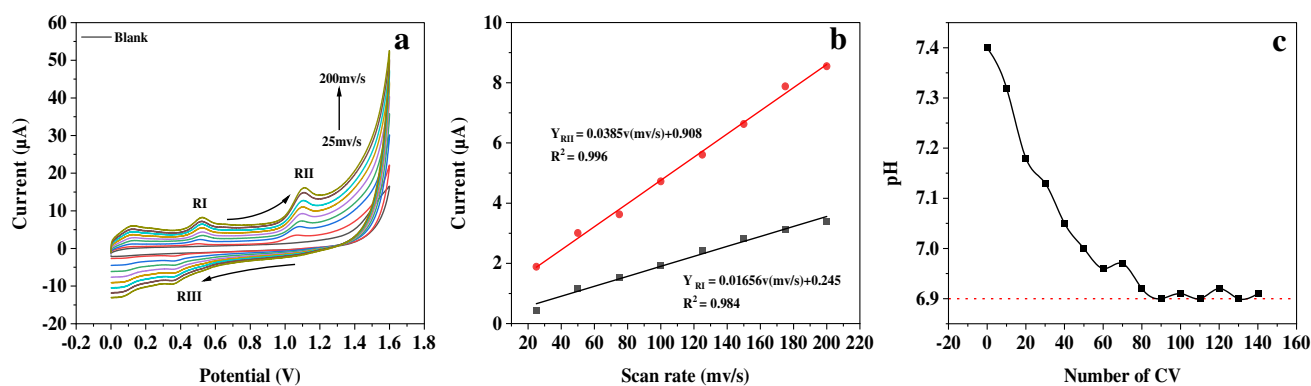
Electrochemical detection of riluzole

During electrochemical measurement in aqueous media, an oxygen reduction reaction is inevitable, which leads to H_2O_2 formation (Eq. 10). In addition, H_2O_2 plays an important role in the electro-oxidation of riluzole. For instance, a study on riluzole as a pollutant treatment has shown that the complete oxidation of riluzole in aqueous solution begins with the opening of the triazole ring, and releases nitrate, sulfate, and fluoride ions. The opening of the triazole ring will generate aromatic substances such as 4-(trifluoromethoxy)aniline (4-TFMA), aniline, and 4-aminophenol (Eq. 11). These aromatic substances will eventually be oxidized to generate CO_2

and water under the action of hydrogen peroxide (as shown in Eq. 12) [56]. In the above process, H_2O_2 plays a key role in electrochemical sensing.
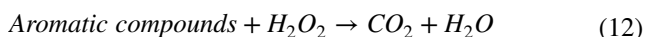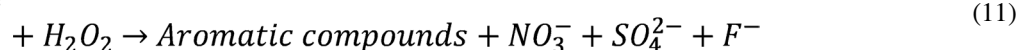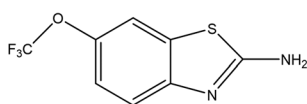
In this work, a GCE was used to detect 25 μmol/L riluzole by CV, and the results are shown in Fig. 4a. It can be clearly seen that riluzole has two oxidation peaks, RI (0.5 V) and RII (1.06 V), and a reduction peak, RIII (0.37 V). The 0.5 V oxidation peak RI and 0.37 V reduction peak RIII form a pair of redox peaks. Related research [57] shows that this pair of redox peaks corresponds to the process of the riluzole molecule releasing fluoride ions and oxidizing methoxy group benzene under electrochemical conditions, while the oxidation peak RII at 1.06 V corresponds to an irreversible oxidation process, due to the opening of the triazole ring and the oxidation of 2-aminothiazole releasing nitrate, sulfate, etc.
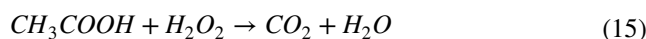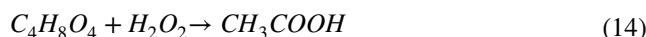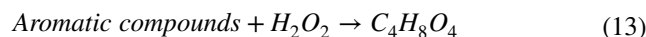
$$O_2 + 2H^+ + 2e^- \rightarrow H_2O_2 \qquad (10)$$

Fig. 4 Electrochemical detection plot of riluzole: (**a**) the cyclic voltammogram of riluzole in PBS solution (pH = 7.4), potential range 0–1.6 V; (**b**) linear fit between oxidation peak I–II and scan rate; (**c**) plot of the relationship between the number of CV and the pH of the solution

$$+\ H_2O_2 \rightarrow Aromatic\ compounds + NO_3^- + SO_4^{2-} + F^- \tag{11}$$

$$Aromatic\ compounds + H_2O_2 \rightarrow CO_2 + H_2O \tag{12}$$

Next, taking two oxidation processes as examples, the electrode kinetics of riluzole were studied by CV. The experimental data are shown in Fig. 4a, and a linear correlation between the oxidation peak current and the scanning rate is shown in Fig. 4b. From Fig. 4b, it can be seen that there is strong linearity between oxidation peak current and the scanning rate. $Ip_{RI} = 0.0166v$ (mV/s) + 0.245, $R^2 = 0.984$ for the oxidation peak R_I, and $Ip_{RII} = 0.0385v$ (mV/s) + 0.908, $R^2 = 0.996$, for the oxidation peak R_{II}. Oxidation peak II is the main detection peak of riluzole, which does not have a corresponding reduction peak during the reverse sweep in the CV detection curve, so the main oxidation of riluzole is considered an irreversible electrochemical catalytic oxidation reaction controlled by adsorption. In addition, fluorine ions are hydrolyzed into hydrofluoric acid and

hydroxide ions, which causes the pH to increase. Interestingly, by measuring the pH of riluzole solution after CV with different scanning times, it is found that the solution pH decreases, not increases, and the final pH is about 6.9 (Fig. 4c). This may be due to the further catalytic cracking of the benzene ring structure in the solution by H_2O_2, generating organic acids, as shown in Eqs. (13)–(15) [56], resulting in a decrease in the overall pH of the solution.

$$Aromatic\ compounds + H_2O_2 \rightarrow C_4H_8O_4 \tag{13}$$

$$C_4H_8O_4 + H_2O_2 \rightarrow CH_3COOH \tag{14}$$

$$CH_3COOH + H_2O_2 \rightarrow CO_2 + H_2O \tag{15}$$

In addition, the different concentrations of riluzole were detected by SWV as shown in Fig. 5a, b shows the good

Fig. 5 Detection curves of riluzole at different concentrations: (**a**) SWV detection curve of riluzole at different concentrations, potential range 0.2–1.4 V, $E_s = 4$ mV, pulse amplitude 0.025 V, f = 4 Hz; (**b**) plot of the relationship between riluzole concentration and peak current
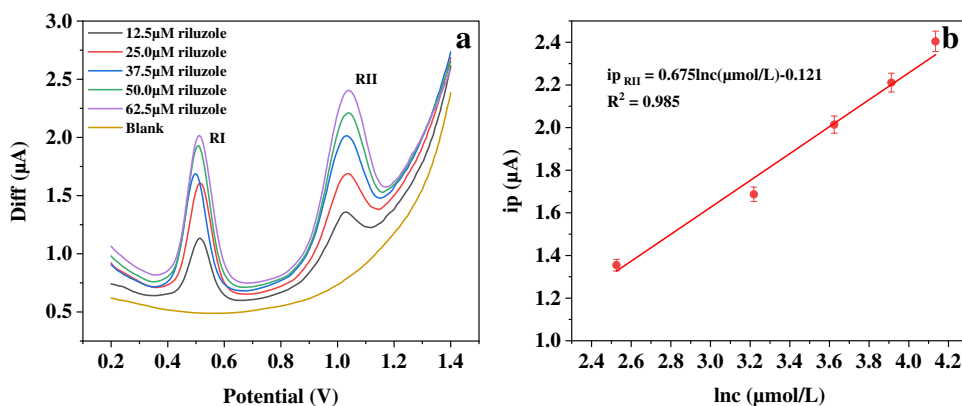
Fig. 6 Effect of riluzole on glutamate under electrochemical conditions: (**a**) the SWV detection plot of 8 mM Glu added with different concentrations of riluzole (0–25 μM) in PBS solution (pH = 7.4), potential range 0–1.4 V, E_s = 4 mV, pulse amplitude 0.025 V, f = 4 Hz; (**b**) curve of the relationship between riluzole concentration and oxidation peaks G_I and R_{II}
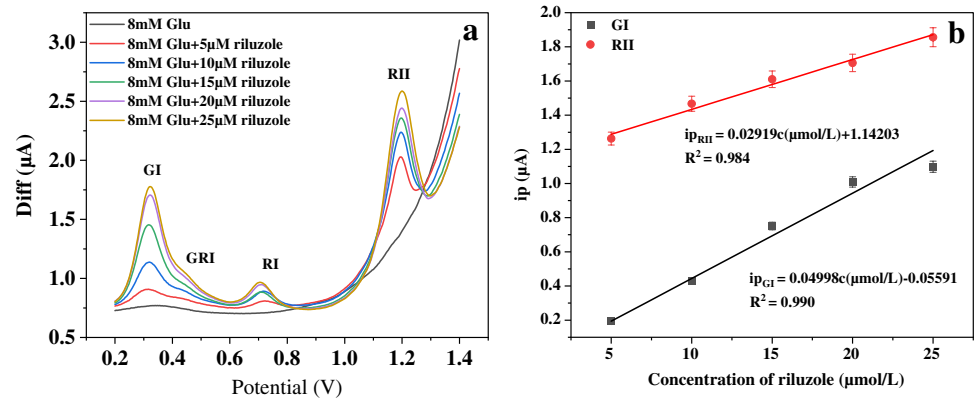

linearity of the currents of riluzole versus concentrations in the range of 12.5–62.5 μmol/L. In order to calculate the detection limit of the GCE for riluzole, the detection characteristic peak of riluzole–that is, the oxidation peak II–was used as the main peak of the riluzole oxidation reaction, and the fitting curve was Ip_{II} (μA) = 0.675lnc (μmol/L)–0.121, R^2 = 0.985, where its slope is defined as the sensitivity coefficient (N) of the sensor. The sensitivity can be obtained by the ratio of N to the electrode surface area, and the sensitivity of GCE to riluzole reaches 9.55 μ A/cm²·μM, using the detection limit calculation formula $Ip_{II} = Ip_0 + 2S$, where $S = 2.833 \times 10^{-7}$A, and $Ip_0 = 9.592 \times 10^{-7}$A for the blank sample. Substitution results in a value of $Ip_{II} = 1.52571 \times 10^{-6}$A. When this value is inserted into the above concentration current linear fitting curve, it can be

concluded that the detection limit of the GCE for riluzole is about 11.47 μmol/L. This is close to the average plasma concentration for riluzole, indicating the potential for drug monitoring [34].

The interaction between riluzole and glutamate under electrochemical conditions

In vivo, riluzole regulates the glutamate system by affecting Glu-related receptors [44–47], but there is no consensus on whether riluzole can directly interact with Glu. In this work, in order to investigate the effect of riluzole on the electrochemical detection of Glu, SWV was used to study the interaction between the two substances. As shown in Fig. 6a, for the Glu-free riluzole solution, a glutamate oxidation peak G_I
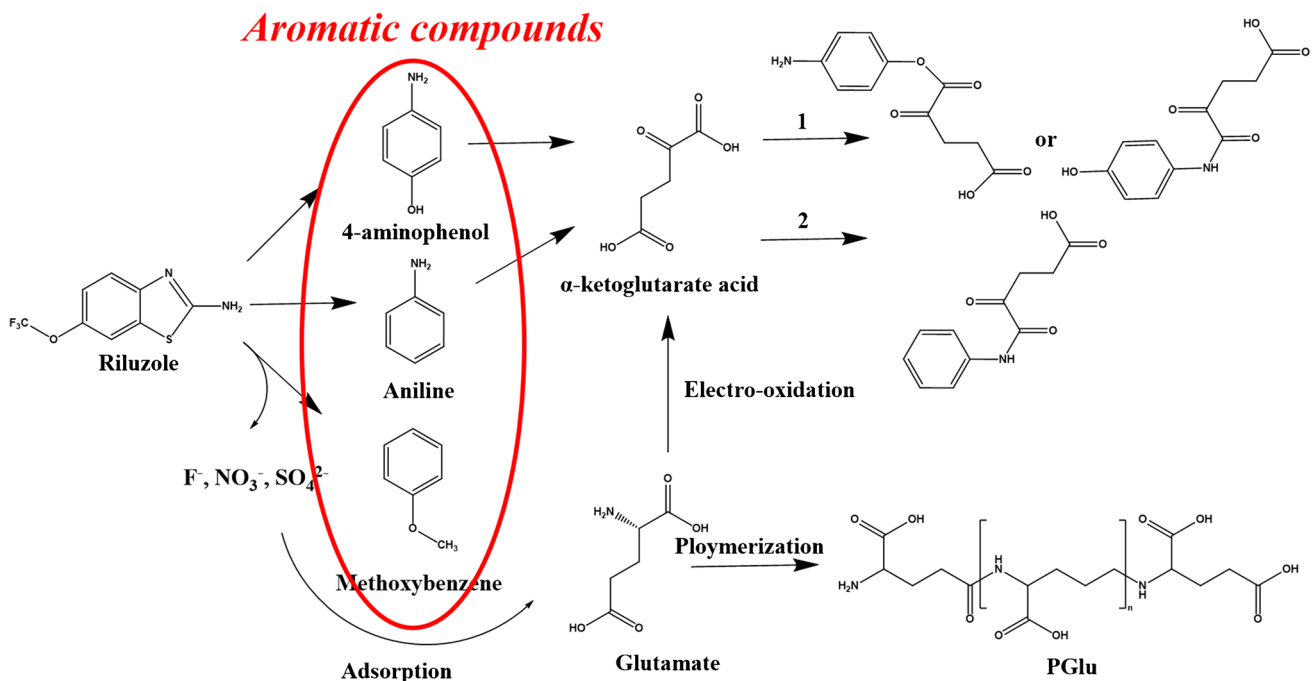
Scheme 2 Effect of riluzole oxidation products on glutamate oxidation products under electrochemical conditions

obviously appeared at 0.33 V. Then the riluzole solution was added into the above Glu solution, and the concentration of riluzole in the entire detection system was increased from 5 μM to 25 μM, with a concentration gradient of 5 μM. In addition to the glutamate oxidation peak G_I, two oxidation peaks R_I and R_{II} were observed at 0.7 V and 1.1 V, respectively, corresponding to the electro-oxidation of riluzole. Compared with the oxidation peak of riluzole solution alone (Fig. 5a), the two oxidation peaks of riluzole in the mixed solution (Fig. 6a) both moved 0.2 V toward a higher potential, which indicates that in this system, its oxidation reaction does not occur as easily as that in the absence of Glu. And compared to the same concentration (25 μmol/L), the area of the oxidation peaks R_{II} of riluzole in Fig. 5a is approximately 536.6 mA· V larger than that of the mixed solution of riluzole in Fig. 6a. This may be due to the presence of Glu, which leads to a more intense oxidation reaction of the oxidation peak R_{II}. With the increase in the concentration of riluzole in the system, the peak current of the oxidation peak G_I shows a linear upward relationship with the concentration of riluzole, corresponding to $Ip_{GI} = 0.04998C$ (μmol/L)–0.05591, $R^2 = 0.990$ (black line in Fig. 6b). Additionally, the oxidation peak III with better linearity is used as the characteristic peak of riluzole, $Ip_{RII} = 0.02919C$ (μmol/L) + 1.14203, $R^2 = 0.984$ for the riluzole within the concentration range of 5–25 μM (red line in Fig. 6b). It can be seen from Fig. 6b that with the increase in the concentration of riluzole, the oxidation peak current of Glu and the concentration of riluzole show a highly linear fit, which further verifies that riluzole may promote the oxidation reaction of Glu under electrochemical conditions; that is, the presence of riluzole can accelerate the oxidation conversion or consumption of Glu. In this work, we found that the glutamate oxidation was not affected by the other interferences including serine, glycine, and aspartate (see ESI† S1). In addition, when the concentration of riluzole is relatively low, a shoulder peak GR_I appears after the oxidation peak G_I, indicating an electrochemical interaction between the two to generate new substances. With the further increase in the concentration of riluzole, the shoulder peak GR_I is covered by the rapidly growing oxidation peak G_I. The stability and repeatability of the sensor are shown in ESI† S2.

Here, from the perspective of the molecular structure of the oxidation product of glutamate and the oxidation product of riluzole (Scheme 2), it can be seen that α-ketoglutaric acid (the oxidation product of Glu) can react with aromatic intermediates during the oxidation reaction of the riluzole, as shown in Scheme 2, reactions (1)–(2). The main reaction is esterification or dehydration condensation reaction. In the reactant solution with a low concentration, the dominant reaction promoting the oxidation of Glu may be the amino and carboxyl groups carried by α-ketoglutaric acid which undergo dehydration and condensation reactions, shifting the reaction balance of Glu toward the right and catalyzing its oxidation reaction. In addition, some

studies in recent years have shown that fluoride ions will be adsorbed by organic substances in aqueous solution; for example, glutamate can generate polyglutamate (PGlu) under electrochemical conditions, and PGlu has an adsorption effect on fluoride ions [58–60]. This may lead to a decrease in the concentration of fluoride ions in the solution, as shown in reaction (3) in Scheme 2, which can cause the oxidation reaction of riluzole to shift to the right, and promote the electrochemical redox of riluzole, thus leading to an increase in the oxidation peaks G_I, R_I, R_{II}, and the shoulder peak GR_I as shown in Fig. 6a.

Conclusions

In conclusion, in this work, electrochemical detection of low-concentration glutamate and the psychotropic drug riluzole was studied using CV and SWV, and the redox reaction mechanism of glutamate under electrochemical conditions was explored. In addition, it was found that under electrochemical conditions, the glutamate inhibitor riluzole may interact with glutamate in aqueous solution and bind to intermediate products, thereby promoting the redox reaction of glutamate.

Author contributions Tao Yu: Writing—original draft, investigation, data curation, visualization, formal analysis. Jingjie Cui: Conceptualization, resources, data curation, software, formal analysis, supervision, methodology, writing—original draft, project administration. Shaowei Chen: Writing—review & editing.

Declarations

References

1. Pál B. Involvement of extrasynaptic glutamate in physiological and pathophysiological changes of neuronal excitability. Cell Mol Life Sci. 2018;75(16):2917–49.
2. Yang SJ, Kim EA, Chang MJ, et al. N-Adamantyl-4-Methylthiazol-2-amine attenuates glutamate-induced oxidative stress and inflammation in the brain. Neurotox Res. 2017;32(1):107–20.
3. Hawkins RA. The blood-brain barrier and glutamate. Am J Clin Nutr. 2009;90(3):867S-874S.
4. Broeders TA, Bhogal AA, Morsinkhof LM, et al. Glutamate levels across deep brain structures in patients with a psychotic disorder and its relation to cognitive functioning. J Psychopharmacol. 2022;36(4):489–97.

5. Hynd MR, Scott HL, Dodd PR. Glutamate-mediated excitotoxicity and neurodegeneration in Alzheimer's disease. Neurochem Int. 2004;45(5):583–95.

6. Niaz K, Zaplatic E, Spoor J. Extensive use of monosodium glutamate: A threat to public health?. EXCLI J. 2018;17:273–278. Published 2018 Mar 19.

7. Clarke G, O'Mahony S, Malone G, Dinan TG. An isocratic high performance liquid chromatography method for the determination of GABA and glutamate in discrete regions of the rodent brain [published correction appears in J Neurosci Methods. 2007 Sep 30;165(2):320]. J Neurosci Methods. 2007;160(2):223–230.

8. Doong RA, Shih HM. Array-based titanium dioxide biosensors for ratiometric determination of glucose, glutamate and urea. Biosens Bioelectron. 2010;25(6):1439–46.

9. Andersen JV, Markussen KH, Jakobsen E, et al. Glutamate metabolism and recycling at the excitatory synapse in health and neurodegeneration. Neuropharmacology. 2021;196:108719.

10. Castillo J, Dávalos A, Naveiro J, Noya M. Neuroexcitatory amino acids and their relation to infarct size and neurological deficit in ischemic stroke. Stroke. 1996;27(6):1060–5.

11. Zauner A, Bullock R, Kuta AJ, Woodward J, Young HF. Glutamate release and cerebral blood flow after severe human head injury. Acta Neurochir Suppl. 1996;67:40–4.

12. Andreadou E, Kapaki E, Kokotis P, et al. Plasma glutamate and glycine levels in patients with amyotrophic lateral sclerosis. In Vivo. 2008;22(1):137–41.

13. Stragierowicz J, Daragó A, Brzeźnicki S, Kilanowicz A. Optimization of ultra-performance liquid chromatography (UPLC) with fluorescence detector (FLD) method for the quantitative determination of selected neurotransmitters in rat brain. Optimization of ultra-performance liquid chromatography (UPLC) with fluorescence detector (FLD) method for the quantitative determination of selected neurotransmitters in rat brain. Med Pr. 2017;68(5):583–91.

14. Campos CDM, Reyes FGR, Manz A, da Silva JAF. On-line electroextraction in capillary electrophoresis: Application on the determination of glutamic acid in soy sauces. Electrophoresis. 2019;40(2):322–9.

15. Kim S, Okazaki S, Otsuka I, et al. Searching for biomarkers in schizophrenia and psychosis: Case-control study using capillary electrophoresis and liquid chromatography time-of-flight mass spectrometry and systematic review for biofluid metabolites. Neuropsychopharmacol Rep. 2022;42(1):42–51.

16. Lorenzo MP, Valiente L, Buendia I, Gortázar AR, Garcia A. Optimization and validation of a chiral CE-LIF method for quantitation of aspartate, glutamate and serine in murine osteocytic and osteoblastic cells. J Chromatogr B Analyt Technol Biomed Life Sci. 2020;1152:122259.

17. Moroz LL, Sohn D, Romanova DY, Kohn AB. Microchemical identification of enantiomers in early-branching animals: Lineage-specific diversification in the usage of D-glutamate and D-aspartate. Biochem Biophys Res Commun. 2020;527(4):947–52.

18. Ta HY, Collin F, Perquis L, Poinsot V, Ong-Meang V, Couderc F. Twenty years of amino acid determination using capillary electrophoresis: A review. Anal Chim Acta. 2021;1174:338233.

19. Qu WJ, Liu T, Chai Y, et al. Efficient detection of L-aspartic acid and L-glutamic acid by self-assembled fluorescent microparticles with AIE and FRET activities. Org Biomol Chem. 2023;21(19):4022–4027. Published 2023 May 17.

20. Xu Z, Ruisong W, Ligong C. Glucosamine modified near-infrared cyanine as a sensitive colorimetric fluorescent chemosensor for aspartic and glutamic acid and its applications. New J Chem. 2014;38(10):4791–8.

21. Ohkuma M, Kaneda M, Yoshida S, Fukuda A, Miyachi E. Optical measurement of glutamate in slice preparations of the mouse retina. Neurosci Res. 2018;137:23–9.

22. Amouzadeh Tabrizi M. A facile method for the fabrication of the microneedle electrode and its application in the enzymatic determination of glutamate. Biosensors (Basel). 2023;13(8):828. Published 2023 Aug 18.

23. Bermingham KP, Doran MM, Bolger FB, Lowry JP. Design optimisation and characterisation of an amperometric glutamate oxidase-based composite biosensor for neurotransmitter l-glutamic acid. Anal Chim Acta. 2022;1224:340205.

24. Maity D, Kumar RTR. Highly sensitive amperometric detection of glutamate by glutamic oxidase immobilized Pt nanoparticle decorated multiwalled carbon nanotubes(MWCNTs)/polypyrrole composite. Biosens Bioelectron. 2019;130:307–14.

25. Özel RE, Ispas C, Ganesana M, Leiter JC, Andreescu S. Glutamate oxidase biosensor based on mixed ceria and titania nanoparticles for the detection of glutamate in hypoxic environments. Biosens Bioelectron. 2014;52:397–402.

26. Liang B, Zhang S, Lang Q, Song J, Han L, Liu A. Amperometric L-glutamate biosensor based on bacterial cell-surface displayed glutamate dehydrogenase. Anal Chim Acta. 2015;884:83–9.

27. Gomes SP, Doležalová J, Araújo AN, et al. Glutamate sol-gel amperometric biosensor based on co-immobilised NADP+ and glutamate dehydrogenase. J Anal Chem. 2013;68:794–800.

28. Martínez-Periñán E, Domínguez-Saldaña A, Villa-Manso AM, Gutiérrez-Sánchez C, Revenga-Parra M, Mateo-Martí E, Pariente F, Lorenzo E. Azure A embedded in carbon dots as NADH electrocatalyst: development of a glutamate electrochemical biosensor. Sensors Actuators B: Chem. 2023;374:132761.

29. Zhenqing D, Junli G, Tiantian S, Jinfeng W, Zhida G, Yanyan S. Nature-inspired mineralization of a wood membrane as a sensitive electrochemical sensing device for in situ recognition of chiral molecules. Green Chem. 2021;23:8685–93.

30. Hughes G, Pemberton RM, Fielden PR, Hart JP. Trends Anal Chem. 2016;79:106–13.

31. Jörissen L. Bifunctional oxygen/air electrodes. J Power Sources. 2006;155(1):23–32.

32. Abdel-Aziz AM, Hassan HH, Badr IHA. Activated glassy carbon electrode as an electrochemical sensing platform for the determination of 4-nitrophenol and dopamine in real samples. ACS Omega. 2022;7(38):34127–35.

33. Zarate CA, Manji HK. Riluzole in psychiatry: a systematic review of the literature. Expert Opin Drug Metab Toxicol. 2008;4(9):1223–34.

34. Groeneveld GJ, van Kan HJ, Lie-A-Huen L, Guchelaar HJ, van den Berg LH. An association study of riluzole serum concentration and survival and disease progression in patients with ALS. Clin Pharmacol Ther. 2008;83(5):718–22.

35. Zarate CA Jr, Quiroz JA, Singh JB, et al. An open-label trial of the glutamate-modulating agent riluzole in combination with lithium for the treatment of bipolar depression. Biol Psychiatry. 2005;57(4):430–2.

36. Debove C, Zeisser P, Salzman PM, Powe LK, Truffinet P. The Rilutek (riluzole) Global Early Access Programme: an open-label safety evaluation in the treatment of amyotrophic lateral sclerosis. Amyotroph Lateral Scler Other Motor Neuron Disord. 2001;2(3):153–8.

37. Sanacora G, Kendell SF, Levin Y, et al. Preliminary evidence of riluzole efficacy in antidepressant-treated patients with residual depressive symptoms. Biol Psychiatry. 2007;61(6):822–5.

38. Chéramy A, Barbeito L, Godeheu G, Glowinski J. Riluzole inhibits the release of glutamate in the caudate nucleus of the cat in vivo. Neurosci Lett. 1992;147(2):209–12.

39. Carbone M, Duty S, Rattray M. Riluzole elevates GLT-1 activity and levels in striatal astrocytes. Neurochem Int. 2012;60(1):31–8.

40. Martin D, Thompson MA, Nadler JV. The neuroprotective agent riluzole inhibits release of glutamate and aspartate from slices of hippocampal area CA1. Eur J Pharmacol. 1993;250(3):473–6.

41. Du J, Suzuki K, Wei Y, et al. The anticonvulsants lamotrigine, riluzole, and valproate differentially regulate AMPA receptor membrane localization: relationship to clinical effects in mood disorders. Neuropsychopharmacology. 2007;32(4):793–802.

42. Fumagalli E, Funicello M, Rauen T, Gobbi M, Mennini T. Riluzole enhances the activity of glutamate transporters GLAST, GLT1 and EAAC1. Eur J Pharmacol. 2008;578(2–3):171–6.

43. Heurteaux C, Laigle C, Blondeau N, Jarretou G, Lazdunski M. Alpha-linolenic acid and riluzole treatment confer cerebral protection and improve survival after focal brain ischemia. Neuroscience. 2006;137(1):241–51.

44. Kumarasamy D, Viswanathan VK, Shetty AP, Pratheep GK, Kanna RM, Rajasekaran S. The role of riluzole in acute traumatic cervical spinal cord injury with incomplete neurological deficit: a prospective, randomised controlled study. Indian J Orthop. 2022;56(12):2160–2168. Published 2022 Oct 5.

45. Cotinat M, Boquet I, Ursino M, et al. Riluzole for treating spasticity in patients with chronic traumatic spinal cord injury: Study protocol in the phase ib/iib adaptive multicenter randomized controlled RILUSCI trial. PLoS One. 2023;18(1):e0276892. Published 2023 Jan 20.

46. Atabak N, Saeed KS, Ali SK, Davood F. The effect of Riluzole on neurological outcomes, blood-brain barrier, brain water and neuroinflammation in traumatic brain injury. Brain Disorders. 2022;8:100052.

47. Obinu MC, Reibaud M, Blanchard V, Moussaoui S, Imperato A. Neuroprotective effect of riluzole in a primate model of Parkinson's disease: behavioral and histological evidence. Mov Disord. 2002;17(1):13–9.

48. Bensimon G, Ludolph A, Agid Y, et al. Riluzole treatment, survival and diagnostic criteria in Parkinson plus disorders: the NNIPPS study. Brain. 2009;132(Pt 1):156–71.

49. Ali MY, Knight D, Howlader MMR. Nonenzymatic electrochemical glutamate sensor using copper oxide nanomaterials and multiwall carbon nanotubes. Biosensors (Basel). 2023;13(2):237. Published 2023 Feb 7.

50. Chi X, Tang Y, Zeng X. Electrode reactions coupled with chemical reactions of oxygen, water and acetaldehyde in an ionic liquid: new approaches for sensing volatile organic compounds. Electrochim Acta. 2016;216:171–80.

51. Sugiyama K, Watanabe K, Komatsu S, et al. Electropolymerization of azure A and pH sensing using poly(azure A)-modified electrodes. Anal Sci. 2021;37(6):893–6.

52. Laviron E. General expression of the linear potential sweep voltammogram in the case of diffusionless electrochemical systems. J Electroanal Chem Interfacial Electrochem. 1979;101(1):19–28.

53. Alhaji NMI, Mary SSL. Kinetics and mechanism of oxidation of glutamic acid by N-bromophthalimide in aqueous acidic medium. E J Chem. 2011;8(4):1472–7.

54. Zhou YQ, Wang NX, Xing Y, et al. Stable acyclic aliphatic solid enols: synthesis, characterization, X-ray structure analysis and calculations. Sci Rep. 2013;3:1058.

55. Mruga D, Soldatkin O, Paliienko K, et al. Optimization of the design and operating conditions of an amperometric biosensor for glutamate concentration measurements in the blood plasma. Electroanalysis. 2021;33(5):1299–307.

56. Bensalah N, Neily E, Bedoui A, Ahmad MI. Mineralization of riluzole by heterogeneous fenton oxidation using natural iron catalysts. Catalysts. 2023;13(1):68.

57. Atana SEH, Dogan-Topal B, Ozkan AS. Electrochemical characterization and rapid voltammetric determination of riluzole in pharmaceuticals and human serum. Anal Lett. 2011;44(6):976–90.

58. Nasrollahpour H, Naseri A, Rashidi MR, Khalilzadeh B. Application of green synthesized WO3-poly glutamic acid nanobiocomposite for early stage biosensing of breast cancer using electrochemical approach. Sci Rep. 2021;11(1):23994. Published 2021 Dec 14.

59. Alan M, Xiaocheng H, Yue Z, Jifang Y, Liying S, Zhenjiang L. An antifouling electrochemical aptasensor based on poly (glutamic acid) and peptide for the sensitive detection of adenosine triphosphate. Microchem J. 2021;168:106365.

60. González-Aguiñaga E, Pérez-Tavares JA, Patakfalvi R, et al. Amino acid complexes of zirconium in a carbon composite for the efficient removal of fluoride ions from water. Int J Environ Res Public Health. 2022;19(6):3640. Published 2022 Mar 18.